Inorganic Chemistry

ARTICLE

pubs.acs.org/IC

Redox-Rich Spin−Spin-Coupled Semiquinoneruthenium Dimers with Intense Near-IR Absorption

Tanaya Kundu,[†] Biprajit Sarkar,[‡] Tapan Kumar Mondal,[§] Shaikh M. Mobin,[†] Francisco A. Urbanos,[⊥] Jan Fiedler,[∥] Reyes Jiménez-Aparicio,[*,⊥] Wolfgang Kaim,[*,‡] and Goutam Kumar Lahiri[*,†]

[†]Department of Chemistry, Indian Institute of Technology Bombay, Powai, Mumbai 400076, India

[‡]Institut für Anorganische Chemie, Universität Stuttgart, Pfaffenwaldring 55, D-70550 Stuttgart, Germany

[⊥]Departamento de Química Inorgánica, Facultad de Ciencias Químicas, Universidad Complutense, Ciudad Universitaria, E-28040 Madrid, Spain

[∥]J. Heyrovský Institute of Physical Chemistry, v.v.i., Academy of Sciences of the Czech Republic, Dolejškova 3, CZ-18223 Prague, Czech Republic

[§]Department of Chemistry, Jadavpur University, Jadavpur, Kolkata 700032, India

Supporting Information

ABSTRACT: Using the $[RuCl(\mu\text{-tppz})ClRu]^{2+}$ [tppz = 2,3,5,6-tetrakis(2-pyridyl)pyrazine] platform for bridging two *o*-quinone/catecholate two-step redox systems (unsubstituted, Q^n, or 3,5- di-*tert*-butyl-substituted, $DTBQ^n$), we have obtained the stable complexes $[(Q^{\bullet-})Ru^{II}Cl(\mu\text{-tppz})ClRu^{II}(Q^{\bullet-})]$ (**1**) and the structurally characterized $[(DTBQ^{\bullet-})Ru^{II}Cl(\mu\text{-tppz})ClRu^{II}(DTBQ^{\bullet-})]$ (**2**). The compounds exhibit mostly quinone-ligand-based redox activity within a narrow potential range, high-intensity near-IR absorptions ($\lambda_{max} \approx 920$ nm; $\varepsilon > 50\,000\ M^{-1}\ cm^{-1}$), and variable intra- and intermolecular spin−spin interactions. Density functional theory calculations, electron paramagnetic resonance (EPR), and spectroelectrochemical results (UV−vis−near-IR region) for three one-electron-reduction and two one-electron-oxidation processes were used to probe the electronic structures of the systems in the various accessible valence states. EPR spectroscopy of the singly charged doublet species showed semiquinone-type response for $\mathbf{1}^+$, $\mathbf{2}^+$, and $\mathbf{2}^-$, while **1** exhibits more metal based spin, a consequence of the easier reduction of Q as compared to DTBQ. Comparison with the analogous redox series involving a more basic *N*-phenyliminoquinone ligand reveals significant differences related to the shifted redox potentials, different space requirements, and different interactions between the metals and the quinone-type ligands. As a result, the tppz bridge is reduced here only after full reduction of the terminal quinone ligands to their catecholate states.

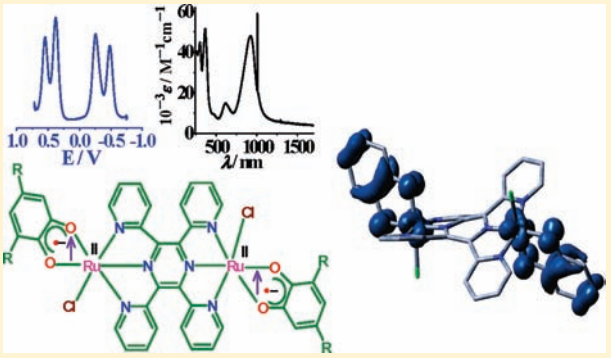

INTRODUCTION

Multielectron reactivity of metal complex arrangements is essential for many small-molecule activating systems in biochemistry (e.g., N_2 fixation, O_2 generation and conversion, CO_2/CH_4 activation)[1] and in corresponding biomimetic constructions.[2] The interaction between individual electron-transfer components is crucial for the functioning of such composite structures. Prominent among the electroactive components are transition metals with several stable oxidation states and organic molecules, typically π systems, with multistep electron-transfer capacity and therefore noninnocent ligand behavior.[3] In addition to multiple ground-state electron-transfer processes, such composite redox systems are susceptible to spin−spin interaction of paramagnetic forms[4] and low-energy optical absorption because of decreased highest occupied molecular orbital (HOMO)−lowest unoccupied molecular orbital (LUMO) energy gaps.[5] New near-IR (NIR)-active compounds are of increasing interest in the areas of information processing, energy research, and analytical and medical applications.[6]

Using the well-characterized, chemically robust, and well-employed[7] $[RuCl(\mu\text{-tppz})ClRu]^{2+}$ bridging platform, we have now managed to couple two *o*-quinone/*o*-semiquinone/catecholate two-step redox systems, the unsubstituted parent, Q^n, and the widely used[8] 3,5-di-*tert*-butyl derivative, $DTBQ^n$, to yield the stable neutral complex $[(Q)RuCl(\mu\text{-tppz})ClRu(Q)]$ (**1**) and the structurally characterized $[(DTBQ)RuCl(\mu\text{-tppz})ClRu(DTBQ)]$ (**2**).

Received: November 13, 2010
Published: April 25, 2011

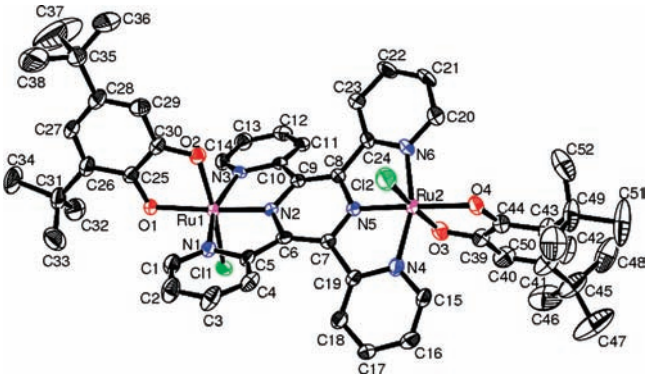

Figure 1. ORTEP diagram of molecule **2** from the crystal. Ellipsoids are drawn at the 50% probability level. Solvents of crystallization and hydrogen atoms are removed for clarity.

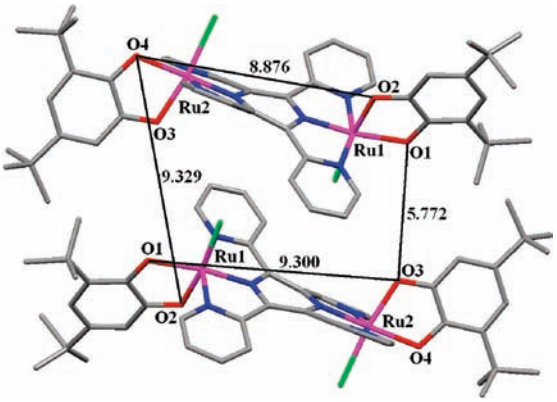

Figure 2. Distance between two catecholate units within two adjacent molecules in the crystal of **2**: O1−O3 = 5.772 Å (all other O···O distances >8.8 Å).

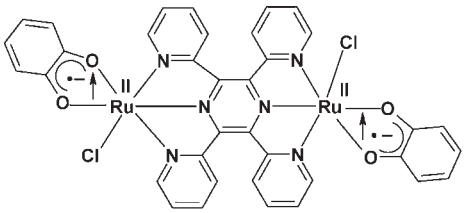

1

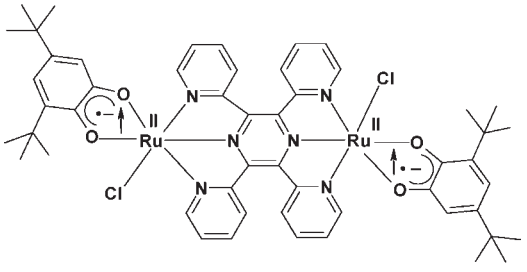

2

Owing to the noninnocent ligand potential of quinones,[3] there are generally several reasonable oxidation state alternatives within complexes containing one or more ruthenium and quinone-type ligands,[7,9] with their assignment often depending on more than one experimental method in conjunction with theoretical support.[10] However, ruthenium complexes with noninnocent ligands such as quinone-type organic molecules are interesting not only for their electron distribution but also for their catalytic potential resulting from the particular electronic situation.[11]

Table 1. Crystallographic Data for $2\cdot CH_2Cl_2\cdot 1.25H_2O$

mol formula	$C_{53}H_{58}Cl_4N_6O_{5.25}Ru_2$
fw	1206.99
cryst syst	monoclinic
space group	$C2/c$
a (Å)	43.1908(7)
b (Å)	12.1729(2)
c (Å)	21.9408(4)
β (deg)	102.241(2)
V (Å^3)	11273.3(3)
Z	8
μ (mm^{-1})	0.775
T (K)	150(2)
D_{calcd} (g cm^{-3})	1.422
$F(000)$	4928
2θ range (deg)	3.35−25.00
data/restraints/param	9891/0/652
R1, wR2 [$I>2\sigma(I)$]	0.0712, 0.1738
R1, wR2 (all data)	0.0934, 0.1810
GOF	1.087
largest diff peak/hole (e Å^{-3})	1.951/−1.592

RESULTS AND DISCUSSION

Synthesis and Identification. Compounds **1** and **2** were obtained from the precursor $[Cl_3Ru^{III}(\mu\text{-tppz})Ru^{III}Cl_3]$ using the corresponding catechol derivatives H_2Q and H_2(DTBQ). In both cases, the reactions led to the exclusive isolation and spectroscopic observation of one isomer. As authenticated by its crystal structure, **2** has the two Ru−Cl groups in an anti configuration. Although there is no structural evidence available, the similar physical data of **1** and **2** (vide infra) suggest that **1** was also obtained in the anti configuration like the *N*-phenylimino analogue $[(Q)RuCl(\mu\text{-tppz})ClRu(Q)]^n$ (**3**^{n}, Q = 4,6-di-*tert*-butyl-*N*-phenyl-*o*-iminobenzoquinone).[7c] The paramagnetic and electrically nonconducting **1** and **2** exhibit satisfactory microanalytical data and display molecular ion peaks at m/z 877.03 and 1101.83, respectively, in CH_3CN, corresponding to the calculated molecular masses of 877.93 (**1**$^+$) and 1102.18 (**2**$^+$) (Figure S1 in the Supporting Information). Paramagnetic **1** and **2** exhibit broad ^{1}H NMR resonances over a wide chemical shift range, from +23 to −38 ppm in $CDCl_3$, resulting from a paramagnetic contact shift[12] (Figure S2 in the Supporting Information).

The typical[7] nonplanarity of the tppz bridging ligand is illustrated by the crystal structure of **2** (Figures 1 and 2 and Tables 1 and 2), with the pyridyl groups alternately displaced upward and downward around the central twisted[7i] pyrazine ring. This configuration has been supported by the density functional theory (DFT)-optimized structure of **1** (Figure S3 in the Supporting Information). For **2**, the experimental dihedral angles between adjacent pyridine rings are 25.8 and 28.7°, and the dihedral angle between the best planes of Ru1−N1−N2−N3 and Ru2−N4−N5−N6 is 30.4°. The appreciably shorter Ru−N(pyrazine,tppz) bond of 1.922(6) Å (average) compared to the

dx.doi.org/10.1021/ic102280q |*Inorg. Chem.* 2011, 50, 4753–4763

Table 2. Selected Bond Distances (Å) and Bond Angles (deg) for 2

bond distances		bond angles	
Ru1−N2	1.922(5)	N2−Ru1−O2	94.1(2)
Ru1−O2	2.009(5)	N2−Ru1−N1	79.9(2)
Ru1−N1	2.037(6)	O2−Ru1−N1	95.0(2)
Ru1−O1	2.048(4)	N2−Ru1−O1	171.9(2)
Ru1−N3	2.079(5)	O2−Ru1−O1	79.46(18)
Ru1−Cl1	2.365(2)	N1−Ru1−O1	95.7(2)
Ru2−N5	1.921(6)	N2−Ru1−N3	80.1(2)
Ru2−N4	2.023(7)	O2−Ru1−N3	87.99(19)
Ru2−O3	2.030(6)	N1−Ru1−N3	159.9(2)
Ru2−O4	2.035(5)	O1−Ru1−N3	104.4(2)
Ru2−N6	2.047(7)	N2−Ru1−Cl1	92.50(17)
Ru2−Cl2	2.388(3)	O2−Ru1−Cl1	172.80(13)
O1−C25	1.306(8)	N1−Ru1−Cl1	88.89(16)
O2−C30	1.309(8)	O1−Ru1−Cl1	94.16(13)
O3−C39	1.308(9)	N3−Ru1−Cl1	90.40(15)
O4−C44	1.307(9)	N5−Ru2−N4	80.8(2)
C25−C26	1.427(10)	N5−Ru2−O3	98.9(2)
C25−C30	1.429(10)	N4−Ru2−O3	91.2(2)
C26−C27	1.373(11)	N5−Ru2−O4	178.2(2)
C27−C28	1.409(12)	N4−Ru2−O4	98.5(2)
C28−C29	1.360(11)	O3−Ru2−O4	79.5(2)
C29−C30	1.413(10)	N5−Ru2−N6	79.5(2)
C39−C40	1.398(11)	N4−Ru2−N6	160.3(2)
C39−C44	1.429(11)	O3−Ru2−N6	91.8(2)
C40−C41	1.366(12)	O4−Ru2−N6	101.2(2)
C41−C42	1.410(13)	N5−Ru2−Cl2	88.7(2)
C42−C43	1.374(12)	N4−Ru2−Cl2	86.58(19)
C43−C44	1.427(10)	O3−Ru2−Cl2	171.69(16)
		O4−Ru2−Cl2	92.89(15)
		N6−Ru2−Cl2	93.0(2)

Ru−N(pyridine,tppz) distance of 2.047(6) Å (average) implies strong (dπ)Ru^{II} → (pπ^*)pyrazine(tppz) back-donation.

The sensitive C−O and C−C(meta) bond distances[9j] involving the catecholate rings [C25−O1, 1.306(8) Å; C30−O2, 1.309(8) Å; C39−O3, 1.308(9) Å; C44−O4, 1.307(9) Å; C26−C27, 1.373(11) Å; C40−C41, 1.366(12) Å] establish the *o*-semiquinone state of the terminal ligands in **2**,[13] based on an established correlation[3c,13] of C−O (ca. 1.31 Å) and intraring C−C bond distances (ca. 1.37 Å for the "meta" bonds[9j,13]) with the *o*-semiquinonato oxidation state. This correlation suggests an oxidation state configuration of **2** as [(DTBQ$^{\bullet-}$)Ru^{II}Cl(μ-tppz)-ClRu^{II}(DTBQ$^{\bullet-}$)]; the DFT-calculated bond distances for **1** also imply the *o*-semiquinone state of the noninnocent terminal ligand (Table S1 in the Supporting Information).

The structurally established configuration and arrangement in the crystal (Figures 1 and 2) raises the question of electronic, magnetic, and electrochemical coupling of the two remote (ca. 1 nm distance) but coordinatively and conjugatively coupled *o*-quinone redox systems.

Magnetism. The paramagnetic compounds **1** and **2** exhibit different magnetic behavior. For complex **2**, the magnetic susceptibility between 300 and 2 K measured at 1 T increases with decreasing temperature (Figure 3). The magnetic moment at room temperature is 2.36 μ_B, i.e., close to the expected value

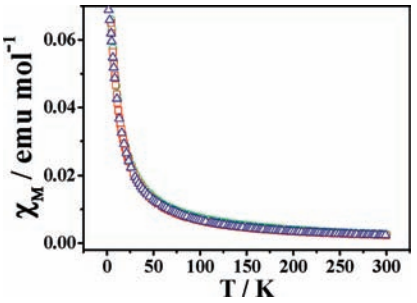

Figure 3. Temperature dependence of the magnetic susceptibility of complex **2**, measured under magnetic fields of 0.1 T (circles, green), 1 T (squares, red), and 5 T (triangles, blue).

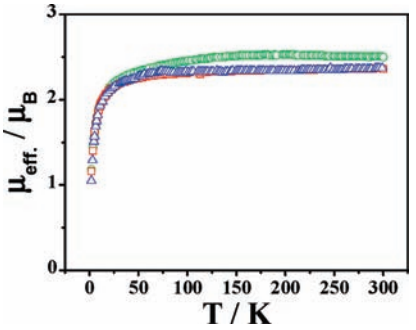

Figure 4. Temperature dependence of the magnetic moment of complex **2**, measured at magnetic fields of 0.1 T (circles, green), 1 T (squares, red), and 5 T (triangles, blue).

for two noninteracting $S = {}^1/_2$ spins per molecule. The magnetic moment smoothly decreases from room temperature to 25 K and then quickly decreases until 2 K (Figure 4). These features are characteristic of weak antiferromagnetic interactions. On the other hand, the magnetization versus magnetic field plot at 300 K is linear (Figure S4 in the Supporting Information), although a slight variation from linearity is observed at high-magnetic-field values at 2 K (Figure S5 in the Supporting Information). The linearity of the magnetization dependence on the magnetic field allows for the use of several models to fit the experimental data.

In a first approximation, it seems reasonable to consider each molecule as a system with two noninteracting $S = {}^1/_2$ spins. Thus, the Bleaney−Bowers equation[14] based on the spin Hamiltonian $H = -JS_1S_2$ ($S_1 = S_2 = {}^1/_2$) can be used to fit the experimental magnetic data of **2**. Additionally, a temperature-independent paramagnetism (TIP) term and the presence of a paramagnetic impurity (P) have been added to the Bleaney−Bowers equation (eq 1).

$$\chi_{mol} = \left(\frac{2Ng^2\beta^2}{KT}\frac{1}{3+e^{-J/KT}} + TIP\right)(1-P) + \frac{Ng^2\beta^2}{2KT}P \quad (1)$$

The terms N, g, β, K, J, and T in eq 1 have their usual meaning, and P is the mole fraction of the noncoupled paramagnetic impurity.

A good fit between the experimental and calculated data was obtained using this model (Figure 5). The parameters obtained in the best fits were $g = 1.87$, $J = -9.61$ cm^{-1}, TIP = 2.59×10^{-4} emu mol^{-1}, and $P = 28.85\%$ with σ^2 (agreement factor) = 7.98×10^{-5}.

dx.doi.org/10.1021/ic102280q |*Inorg. Chem.* 2011, 50, 4753–4763

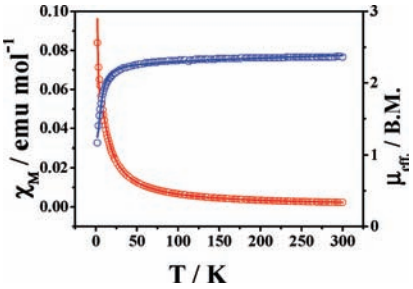

Figure 5. Temperature-dependent experimental (circles) and calculated (solid lines, eq 1) magnetic susceptibility and moment values for complex **2**, under a magnetic field of 1 T.

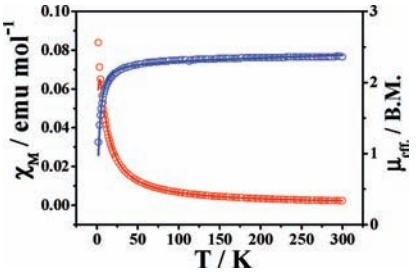

Figure 6. Temperature-dependent experimental (circles) and calculated (solid lines, eq 2) magnetic susceptibility and moment values for complex **2**, under a magnetic field of 1 T.

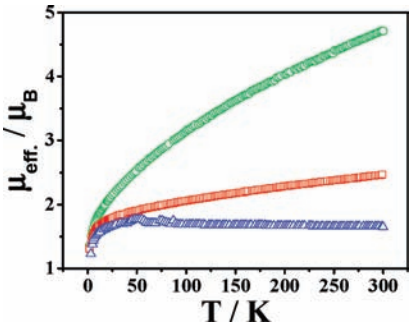

Figure 7. Temperature dependence of the magnetic moment of complex **1**, measured at magnetic fields of 0.1 T (circles, green), 1 T (squares, red), and 5 T (triangles, blue).

The J value of -9.61 cm^{-1} indicates weak intramolecular antiferromagnetic interaction between two $S = {}^1/_2$ spins. The g value is low, and the TIP value is typical for ruthenium compounds[9g,15] but P (28.85%) is too high. The presence of a paramagnetic impurity is usually considered in such fits of the magnetic properties of coordination compounds mainly when the complex displays antiferromagnetic interactions.[9h,16,17] However, in the present case, the high value obtained for the paramagnetic impurity is not reasonable. A related system Zn(tmda)(3,6-DBSQ)$_2$ (tmda = *N*,*N*′,*N*′-tetramethylethylenediamine; 3,6-DBSQ = 3,6-*tert*-butyl-1,2-semiquinonate) with two semiquinone radicals separated by a diamagnetic Zn^{II} ion has been described as containing two noninteracting $S = {}^1/_2$ spins.[18] However, the computational studies of molecule **2** have shown stabilization by 983 cm^{-1} of the triplet ground state over the singlet form, a difference that is higher than the thermal energy at 300 K (209 cm^{-1}) and that therefore suggests that this complex should be considered as an $S = 1$ system.

In order to analyze the magnetic properties of **2** based on an $S = 1$ ground state, we have examined the crystal structure of this complex. Analysis of the structure shows most intramolecular contacts in the *bc* plane, while the shortest relevant *intermolecular* contact was found at 5.77 Å between two spin-bearing semiquinone oxygen atoms, O1 and O3, of different molecules (Figure 2). In the unit cell of crystalline **2**, there are pairs of molecules related by an inversion center. Thus, we have considered the existence of intermolecular interactions between these pairs of molecules with $S = 1$ spin states, and we have used eq 2[19] based on the spin Hamiltonian $H = -JS_1S_2$ ($S_1 = S_2 = 1$) to fit the experimental magnetic data of **2**. Similarly to eq 1, two terms considering TIP and the same expression for the paramagnetic impurity have been added to give the following equation.

$$\chi_{\mathrm{mol}} = \left[\frac{Ng^2\beta^2}{2KT}\,\frac{2e^{J/KT} + 10e^{3J/KT}}{1 + 3e^{J/KT} + 5e^{3J/KT}} + \mathrm{TIP}\right](1 - P) + \frac{Ng^2\beta^2}{2KT}P \qquad (2)$$

The parameters obtained in the best fits (Figure 6) are $g = 1.64$, $J = -3.07$ cm^{-1}, TIP = 2.06×10^{-4} emu mol^{-1}, $P = 7.37\%$, and σ^2 (agreement factor) = 1.22×10^{-4}. The J value of -3.07 cm^{-1} confirms a very weak antiferromagnetic interaction between the two $S = 1$ spins. These parameters are similar to those obtained with eq 1, although with this model, the antiferromagnetic coupling is intermolecular. The calculated paramagnetic impurity is significantly less than that obtained with eq 1.

To determine whether the magnetic behavior of this complex changes with the magnetic field in analogy to other semiquinoneruthenium compounds,[20] we have carried out additional magnetization measurements at variable temperatures under 0.1 and 5 T. The magnetic susceptibility values at 5 T are identical with those obtained under 1 T; however, at 0.1 T, there is a very slight difference (Figure 3). This difference is better observed in the representation of the magnetic moment versus temperature plot (Figure 4), where the magnetic moment at 0.1 T is higher than that calculated at 1 or 5 T. The dependence of the magnetic moment on the magnetic field is compatible with the presence of ferromagnetism in the sample. This ferromagnetism could be due to the presence of ferromagnetic interactions in complex **2** but would also be compatible with the presence of a ferromagnetic impurity. It is well-known that ferromagnetic impurities in paramagnetic complexes can seriously affect the magnetic susceptibility results.[21] If the impurity deduced from the fitting procedure corresponds to a ferromagnetic phase, the higher dependence of the susceptibility could be the cause of the large amount of paramagnetic impurity obtained by the fit. As a consequence, it remains open whether the ferromagnetism observed in this complex is an intrinsic property of the compound or is due to the presence of a ferromagnetic impurity.

The magnetic susceptibility of complex **1** between 300 and 2 K (at 0.5, 1, and 5 T) increases with decreasing temperature (Figure S6 in the Supporting Information) but also shows a dependence on the magnetic field. Similar to complex **2**, this dependence is better observed through variation of the magnetic moment with temperature (Figure 7). As one can observe in this figure, the magnetic moment at 0.1 and 1 T shows a strong decrease with decreasing temperatures, whereas at 5 T, it shows a slight increase

dx.doi.org/10.1021/ic102280q |*Inorg. Chem.* 2011, 50, 4753–4763

Table 3. Electrochemical Data[a]

	$E_{1/2}$ (ΔE_{pp})[b]										
complex	Ox4[c]	Ox3[c]	Ox2	Ox1	Red1	Red2	Red3	Red4[d]	K_{c1}[e,f]	K_{c2}[e,g]	K_{c0}[e,h]
1	1.58	1.41	0.53 (52)	0.37 (53)	−0.27 (59)	−0.52 (60)	−1.24 (53)	−1.77	5.2×10^2	1.7×10^4	7×10^{10}
2	1.50	1.29	0.41 (51)	0.22 (60)	−0.41 (65)	−0.66 (69)	−1.34 (70)	−1.88	1.7×10^3	1.7×10^4	4.8×10^{10}
3	0.89[i]	0.53[i]	−0.78[i]	−0.95[i]	−1.55[i]	−1.84[i]	−2.26[i]		7.9×10^2	7.9×10^4	1.5×10^{10}

[a] From cyclic voltammetry in CH_3CN/0.1 M Et_4NClO_4 at 100 mV s^{-1}. [b] In V versus SCE; peak potential differences ΔE_{pp} [mV] (in parentheses). [c] E_{pa} values for irreversible oxidations. [d] E_{pc} values for irreversible reductions. [e] Comproportionation constant from $RT \ln K_c = nF(\Delta E)$. [f] K_{c1} between Ox1 and Ox2. [g] K_{c2} between Red1 and Red2. [h] K_{c0} between Ox1 and Red1. [i] Corresponding half-wave potentials from ref 7c for **3** recalculated using the value $E_{1/2}(FeCp_2^{+/0}) = +0.40$ V vs SCE.

until about 50 K, followed by a sharp decrease until 2 K. The strong dependence of the magnetic properties on the magnetic field suggests the existence of sizable ferromagnetic interactions. In addition, the decrease of the magnetic moment with temperature indicates the existence of antiferromagnetic coupling. The contribution of a fractional ferromagnetic impurity to the total susceptibility can be corrected using a strong applied magnetic field[22] to ensure saturation of the sample. However, in this case, saturation is not reached at the maximum magnetic field used (5 T), which prevented us from making the mentioned corrections to check whether the source of ferromagnetism is an impurity.

The representation of the magnetization versus magnetic field at 300 and 2 K is not linear, which also suggests the presence of ferromagnetic interactions in **1**, as do the small hysteresis loops at 300 and 2 K (Figures S7 and S8 in the Supporting Information). A similar behavior has been observed in other ruthenium complexes,[20] where, in contrast, saturation of the magnetization was achieved at 300 K.

The zero-field-cooled (ZFC) and field-cooled (FC) thermomagnetization curves at low magnetic field (0.1 T) do not show appreciable irreversibility and, therefore, these measurements do not confirm the formation of a magnetically ordered state. However, this lack of reversibility is in accordance with the low remnant magnetization observed in the hysteresis cycles.

On the other hand, the magnetic moment at room temperature at high magnetic field (5 T) is 1.66 μ_B (Figure 7), which is lower than that expected for two noninteracting $S = {}^1/_2$ spins per molecule and for an $S = 1$ spin system. The computational studies on **1** have shown stabilization (by 4885 cm^{-1}) of the triplet ground state over the singlet form (vide infra). This difference is much higher than that calculated for complex **2**, which indicates that **1** must also be considered as an $S = 1$ system. However, as stated above, the decrease of the magnetic moment with a decrease in the temperature indicates the presence of antiferromagnetic interactions, while variation of the magnetization with the magnetic field and the hysteresis loops confirms the existence of ferromagnetism. Considering a triplet ground state, the antiferromagnetic interaction must then be intermolecular, and the ferromagnetism could be attributed to a spin canting of the $S = 1$ units. Spin canting is usually observed when the local spins in the ordered magnetic state are neither perfectly parallel nor antiparallel but are canted.[22] Spin canting is frequently observed for nonmolecular solids but has also been well documented for coordination compounds.[23] Unfortunately, the nonlinear response of the magnetization toward the applied magnetic field prevented the use of approximations to fit the experimental data.

In any case, the magnetic properties of **1** reveal ferromagnetism at room temperature, hysteresis loops at 300 and 2 K, and the absence of magnetization saturation at 2 or 300 K even at high magnetic fields. Although the presence of a ferromagnetic impurity cannot be completely ruled out, the decrease of the ferromagnetism with decreasing temperature and the observation of ferromagnetism in similar compounds[20] render the ferromagnetism as an intrinsic property of this compound.

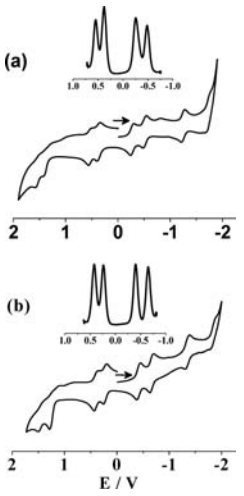

Figure 8. Cyclic voltammograms and differential pulse voltammograms (for the first two oxidized and reduced steps, inset) of (a) **1** and (b) **2** in CH_3CN/0.1 M NEt_4ClO_4 at 298 K. Scan rate: 100 mV s^{-1}.

In summary, complexes **1** and **2** behave as $S = 1$ systems, which interact antiferromagnetically ($J \approx -3$ cm^{-1}) with neighboring molecules. In the case of **1**, the magnetization curves indicate the presence of spin canting, probably due to packing of the molecules in the solid state. For complex **2**, the observed formation of pairs of molecules in the crystal is presumed to be responsible for the total compensation of spins at very low temperatures in the antiferromagnetic state.

Electrochemistry. Complexes **1** and **2** exhibit multiple successive redox processes, four oxidations (Ox1−Ox4) and four reductions (Red1−Red4) within the potential range of ±2 V vs SCE in CH_3CN (Table 3 and Figure 8). The potentials indicate the more facile oxidation of **2** over **1** due to the electron-donating ^{t}Bu substituents. The initial oxidation, Oxl/Ox2, and the first three reduction steps (Red1/Red2/Red3) are fully reversible. The potential separations between Ox1/Ox2 and Red1/Red2 lead to comproportionation constants ($K_c = 5.2 \times 10^2$, 1.7×10^3/1.7×10^4, 1.7×10^4) of about 10^3 and 10^4, respectively, implying a moderate thermodynamic stability of the odd-electron intermediates, $[(Q^0)Ru^{II}Cl(\mu\text{-tppz})ClRu^{II}(Q^{\bullet-})]^+$ ($\mathbf{1}^+/\mathbf{2}^+$) and

dx.doi.org/10.1021/ic102280q |*Inorg. Chem.* 2011, 50, 4753–4763

Scheme 1

$[(Q^{o})Ru^{II}Cl(\mu\text{-tppz})ClRu^{II}(Q^{o})]^{2+}$ or $[(Q^{\bullet-})Ru^{III}Cl(\mu\text{-tppz})ClRu^{III}(Q^{\bullet-})]^{2+}$

$-e^{-}$ $+e^{-}$

$[(Q^{o})Ru^{II}Cl(\mu\text{-tppz})ClRu^{II}(Q^{\bullet-})]^{+}$ or $[(Q^{\bullet-})Ru^{II}Cl(\mu\text{-tppz})ClRu^{III}(Q^{\bullet-})]^{+}$

$-e^{-}$ $+e^{-}$

$[(Q^{\bullet-})Ru^{II}Cl(\mu\text{-tppz})ClRu^{II}(Q^{\bullet-})]$ (Starting Form)

$-e^{-}$ $+e^{-}$

$[(Q^{2-})Ru^{III}Cl(\mu\text{-tppz})ClRu^{II}(Q^{2-})]^{-}$ or $[(Q^{2-})Ru^{II}Cl(\mu\text{-tppz})ClRu^{II}(Q^{\bullet-})]^{-}$ ($\mathbf{2}^{-}$)

$-e^{-}$ $+e^{-}$ ($\mathbf{1}^{-}$)

$[(Q^{2-})Ru^{II}Cl(\mu\text{-tppz})ClRu^{II}(Q^{2-})]^{2-}$

$-e^{-}$ $+e^{-}$

$[(Q^{2-})Ru^{II}Cl(\mu\text{-tppz}^{\bullet-})ClRu^{II}(Q^{2-})]^{3-}$

Table 4. EPR Data[a] of $\mathbf{1}^{n}$ and $\mathbf{2}^{n}$

complex	g_1	g_2	g_3
1	2.06	2.00	2.00
2	2.03[b]	2.00	1.987
$\mathbf{1}^{+}$	2.03	2.00	2.00
$\mathbf{2}^{+}$	2.025	2.00	1.986
$\mathbf{1}^{-}$	2.26	2.095	1.998
$\mathbf{2}^{-}$[c]	2.02	2.00	1.986

[a] From in situ measurements at 110 K in CH_3CN/0.1 M Bu_4NPF_6; electrolytic oxidation and reduction, respectively. [b] Unresolved hyperfine structure. [c] Weak signal also at 300 K.

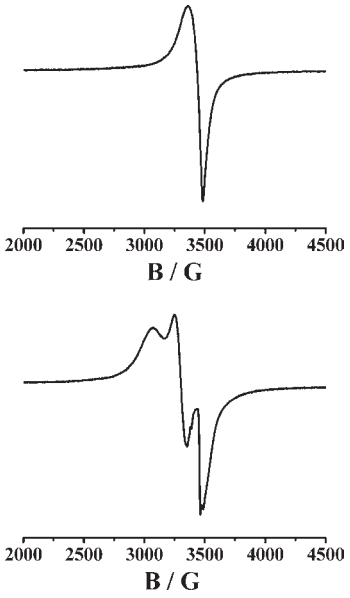

Figure 9. EPR spectra in frozen CH_3CN solutions (110 K) of **1** (top) and $\mathbf{1}^{-}$ (bottom).

$[(Q^{\bullet-})Ru^{II}Cl(\mu\text{-tppz})ClRu^{II}(Q^{2-})]^{-}$ ($\mathbf{1}^{-}/\mathbf{2}^{-}$). The potential separation between the first oxidation (Ox1) and the first reduction (Red1) is only about 0.6 V in both **1** and **2**, leading

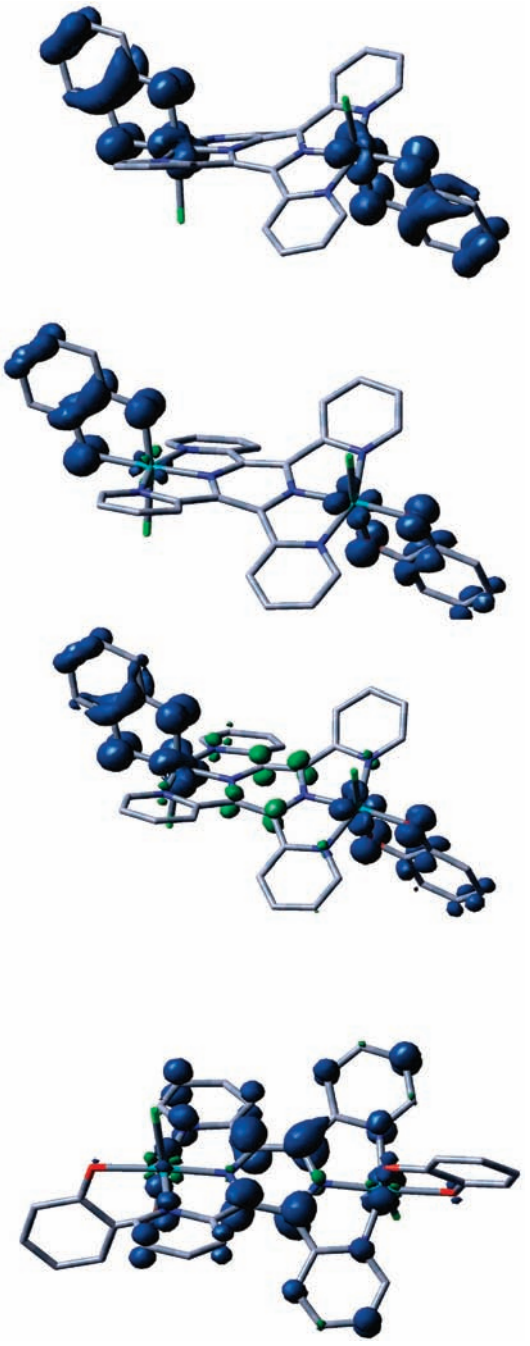

Figure 10. Spin-density plots of **1**, $\mathbf{1}^{+}$, $\mathbf{1}^{-}$, and $\mathbf{1}^{3-}$ (from top to bottom).

Table 5. Spin Densities of Paramagnetic Forms of $\mathbf{1}^{n}$ as Calculated from DFT[a]

	$\mathbf{1}^{b}$	$\mathbf{1}^{+}$	$\mathbf{1}^{-}$	$\mathbf{1}^{3-}$
ruthenium[c]	0.2187	0.0098	0.2646	0.0335
	0.2178	0.0703	0.1195	0.0782
chlorine	0.0115	−0.0139	0.0124	−0.0024
tppz	−0.0349	0.0386	−0.2618	0.8622
quinone[d]	1.5864	0.8813	0.8653	0.0285

[a] From (U)B3LYP calculations. [b] Triplet ground state. [c] Ru1 and Ru2. [d] Quinone/semiquinone/catecholate redox system.

dx.doi.org/10.1021/ic102280q |*Inorg. Chem.* 2011, 50, 4753–4763

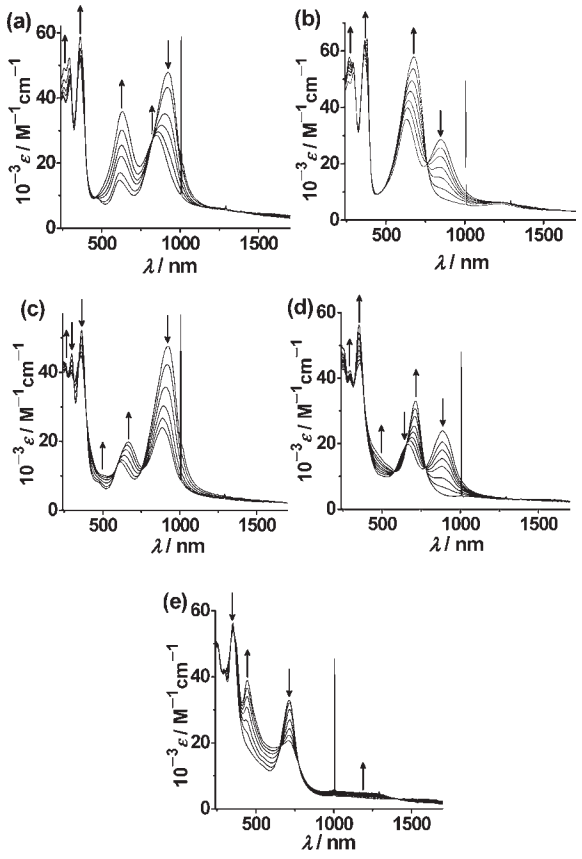

Figure 11. UV−vis−NIR spectroelectrochemistry for the conversions of (a) $\mathbf{1} \rightarrow \mathbf{1}^{+}$, (b) $\mathbf{1}^{+} \rightarrow \mathbf{1}^{2+}$, (c) $\mathbf{1} \rightarrow \mathbf{1}^{-}$, (d) $\mathbf{1}^{-} \rightarrow \mathbf{1}^{2-}$, and (e) $\mathbf{1}^{2-} \rightarrow \mathbf{1}^{3-}$ in CH_3CN/0.1 M Bu_4NPF_6. Signal at 1000 nm from detector switching.

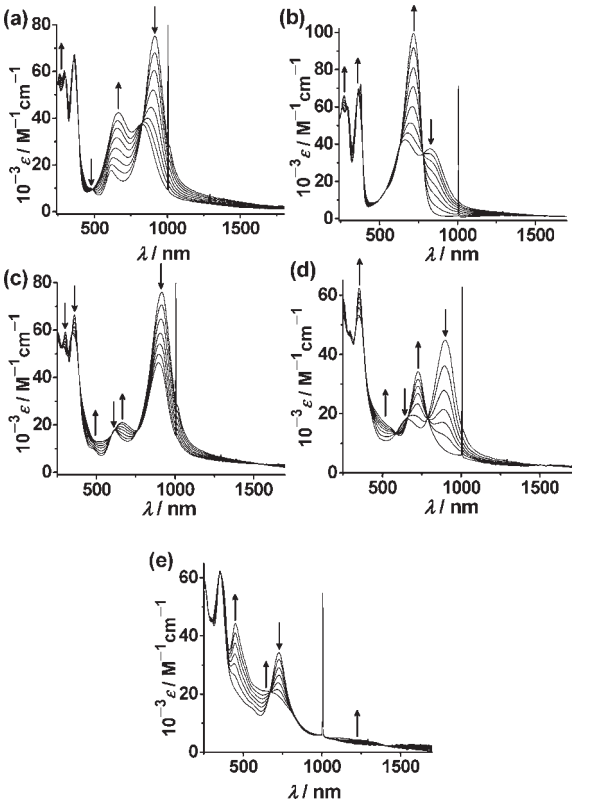

Figure 12. UV−vis−NIR spectroelectrochemistry for the conversions of (a) $\mathbf{2} \rightarrow \mathbf{2}^{+}$, (b) $\mathbf{2}^{+} \rightarrow \mathbf{2}^{2+}$, (c) $\mathbf{2} \rightarrow \mathbf{2}^{-}$, (d) $\mathbf{2}^{-} \rightarrow \mathbf{2}^{2-}$, and (e) $\mathbf{2}^{2-} \rightarrow \mathbf{2}^{3-}$ in CH_3CN/0.1 M Bu_4NPF_6. Signal at 1000 nm from detector switching.

to K_c values of ca. 10^{10}, which are typical for semiquinone intermediates (Figure 8 and Table 3).

The redox series for **1** and **2** (cf. Scheme 1) appears qualitatively similar to that observed for the analogous $[(Q)RuCl(\mu\text{-tppz})ClRu(Q)]^n$ system **3** with Q = 4,6-di-*tert*-butyl-*N*-phenyl-*o*-iminobenzoquinone.[7c] Upon a comparison of **1** and **2** with **3**, it is found that the potentials are 0.6−1.3 V more positive for **1** and **2**, obviously because of the weaker σ-donor and stronger π-acceptor effects of the quinone ligands in **1** and **2** relative to the *N*-phenyliminoquinone ligands in **3**. Accordingly, complexes **1** and **2** were obtained and isolated in their neutral states in contrast to the dicationic forms obtained in the case of **3**.[7c] Despite the rather different values of the redox potentials, the comproportionation constants are of the same order of magnitude as those found for **3** (K_{c1} (monocation) = 7.9×10^2, K_{c2} (monoanion) = 7.9×10^4, and K_{c0} (neutral) = 1.5×10^{10}),[7c] which suggests a similar electron redistribution for corresponding redox steps of **1**−**3**. However, there are more subtle consequences of the alteration of the quinone-type ligands, as is evident from a more detailed inspection. Both the slightly lower K_{c1} and K_{c2} and the higher K_{c0} values for **1** and **2** in comparison to **3** reveal a more pronounced stabilization of the neutral forms in the case of **1** and **2**. Substantial variation of the electron distribution in the monoanionic forms of the complexes is evident from electron paramagnetic resonance (EPR) spectroelectrochemistry (see the next section and the Conclusions section).

EPR Spectroscopy. The EPR results for neutral **1** and **2** as well as for the monooxidized and monoreduced species $\mathbf{1}^{+}$, $\mathbf{2}^{+}$, $\mathbf{1}^{-}$, and $\mathbf{2}^{-}$ are presented in Table 4; Figure 9 shows the representative spectra.

No half-field signals were observed for compounds **1** and **2**. Except for $\mathbf{1}^{-}$, all other signals are nearly axial (Figure 9) with small *g* anisotropy around *g* = 2, signifying only small participation of the 4d metal with its high spin−orbit coupling constant at the singly occupied molecular orbital (SOMO). This is confirmed by DFT spin-density calculations (Figure 10 and Table 5). We attribute this well-established[20] feature to the *o*-semiquinonatoruthenium(II) moiety. The only exception, $\mathbf{1}^{-}$, exhibits a larger *g* anisotropy, with components significantly higher than *g* = 2 (Figure 9 and Table 4), which points to some ruthenium(III) character with the low-spin d^5 configuration.[9] Apparently, the system **1** with the better electron-accepting (unsubstituted) quinone termini Q prefers the metal−metal mixed-valent bis(catecholate) alternative after reduction (Scheme 1), whereas $\mathbf{2}^{-}$ with the more easily oxidizable $DTBQ^{n-}$ stays with the diruthenium(II) arrangement and a partially oxidized catecholate combination, $DTBQ^{\bullet-}/DTBQ^{2-}$ (Scheme 1).

For the monocations $\mathbf{1}^{+}$ and $\mathbf{2}^{+}$, the observed semiquinone-type spin can be interpreted by either formulation from Scheme 1, i.e., $[(Q^0)Ru^{II}Cl(\mu\text{-tppz})ClRu^{II}(Q^{\bullet-})]^{+}$ with a ruthenium(II)/quinone and an EPR-active ruthenium(II)/semiquinone terminus or $[(Q^{\bullet-})Ru^{II}Cl(\mu\text{-tppz})ClRu^{III}(Q^{\bullet-})]^{+}$ with an EPR-inactive[20] ruthenium(III)/semiquinone and one EPR-active ruthenium(II)/semiquinone component. The difference thus lies in the Ru^{II}/Q^0 versus $Ru^{III}/Q^{\bullet-}$ alternative, which is hard to pinpoint[9b,10,20] and best described through a resonance formulation with variable non-negligible contributions from both forms.[10]

dx.doi.org/10.1021/ic102280q |*Inorg. Chem.* 2011, 50, 4753–4763

Table 6. UV−vis−NIR Spectroelectrochemical Data for 1 and 2 in CH_3CN/0.1 M Bu_4NPF_6

complex	λ_{max} [nm] (ε [M^{-1} cm^{-1}])
$\mathbf{1}^{2+}$	679 (58 000), 380 (64 300), 365 (63 800), 292 (sh), 268 (57 800)
$\mathbf{1}^{+}$	849 (28 300), 630 (35 900), 363 (58 600), 294 (52 500), 260 (49 000)
1	925 (47 500), 613 (14 900), 468 (9300), 425 (sh), 362 (51 500), 298 (44 700), 255 (40 400)
$\mathbf{1}^{-}$	885 (24 000), 665 (19 700), 505 (sh), 357 (44 500), 340 (sh), 295 (39 700), 255 (sh)
$\mathbf{1}^{2-}$	714 (33 000), 495 (sh), 353 (56 200), 295 (42 400), 260 (sh)
$\mathbf{1}^{3-}$	1210 (sh, br), 710 (20 700), 446 (38 900), 375 (sh), 354 (53 700), 255 (49 500)
$\mathbf{2}^{2+}$	719 (99 500), 380 (72 300), 364 (69 800), 273 (66 200)
$\mathbf{2}^{+}$	830 (37 500), 665 (42 500), 365 (67 500), 295 (60 300), 262 (59 100)
2	916 (74 000), 615 (17 500), 472 (10 200), 430 (sh), 360 (65 300), 302 (58 200), 252 (55 000)
$\mathbf{2}^{-}$	895 (46 200), 663 (20 900), 510 (sh), 347 (58 200), 290 (sh), 260 (sh)
$\mathbf{2}^{2-}$	728 (34 300), 510 (sh), 352 (62 500), 255 (sh)
$\mathbf{2}^{3-}$	1205 (sh, br), 670 (sh), 449 (44 300), 355 (62 000), 250 (sh)

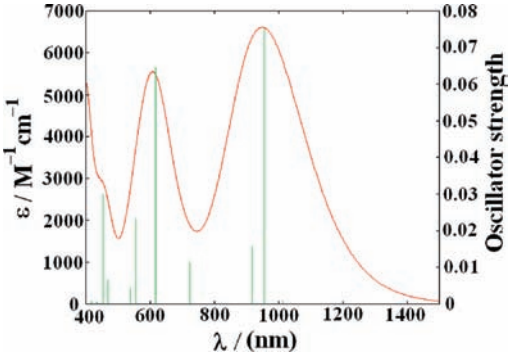

Figure 13. Absorption spectrum of **1** with DFT-calculated transitions.

The DFT-calculated spin densities (Figure 10, Table 5, and Tables S2−S7 in the Supporting Information) agree with the experimental results from EPR spectroscopy (Figure 9 and Table 4). The neutral triplet compound **1** has most of the spin on the semiquinones, as does the oxidized form $\mathbf{1}^{+}$. The monoanion $\mathbf{1}^{-}$, on the other hand, bears a high percentage of spin on the metals, whereas the trianion $\mathbf{1}^{3-}$ is calculated to be a $tppz^{\bullet-}$ radical complex, as deduced experimentally from NIR spectroelectrochemistry (Figures 11e and 12e).

Electronic Transitions and Spectroelectrochemistry. The small difference of only about 0.6 V between the oxidation and reduction potentials of each of the compounds **1** and **2** is reflected by the small frontier orbital energy gap, as calculated by DFT for **1** (Table S2 in the Supporting Information). In agreement with this notion, the compounds exhibit low-energy absorptions in the NIR region, around 920 nm (10 870 cm^{-1}, 1.34 eV), with the bands being characterized by a rather small width ($\Delta\nu_{1/2}$ ca. 1800 cm^{-1}) and very high intensity with $\varepsilon > 50\,000$ M^{-1} cm^{-1} (Figures 11 and 12 and Table 6). The time-dependent DFT (TD-DFT) calculation for **1** predicts an intense absorption at 956 nm, in agreement with the experiment, with the transition involving charge transfer from the periphery (Q, Ru) to the π^*(tppz) core region. Figure 13 depicts the TD-DFT-calculated transitions (Table 7) and the synthesized spectrum of **1**, which agrees well with the experimental spectrum.

Two reversible oxidation and three reversible reduction processes could be monitored by UV−vis−NIR spectroelectrochemistry (Figures 11 and 12 and Table 6). The reversibility and preserved integrity of the electrode-generated redox states during the longer time needed for spectroelectrochemical measurements[24] was proven for all steps through comparison of the starting and final spectra obtained from the cyclic (reduction/reoxidation or oxidation/rereduction) spectroelectrochemical experiments. Similarly, we did not observe any substantial difference in the (spectro)electrochemical behavior of the reversible processes as a function of electrolyte changes, NEt_4^+/NBu_4^+ or ClO_4^-/PF_6^-. Stepwise oxidation results in diminishing intensity and a hypsochromic shift of the NIR band and in the emergence of a very intense band around 700 nm. As outlined in the EPR discussion, the Ru^{II}/Q^0 versus $Ru^{III}/Q^{\bullet-}$ alternative is difficult to establish,[9b,10,20] thus frequently best described through a resonance formulation. Such an interpretation is also suggested for the assignment of the intense long-wavelength bands in $\mathbf{1}^{+}$, $\mathbf{2}^{+}$, $\mathbf{1}^{2+}$, and $\mathbf{2}^{2+}$, which we attribute to mixed (MLCT/LMCT) charge-transfer transitions involving the two formulations Ru^{II}/Q^0 and $Ru^{III}/Q^{\bullet-}$. It may be noted that unreduced *o*-quinones are weakly basic and thus generally labile ligands,[25] while the antiferromagnetically coupled ruthenium(III)/semiquinone entity has been well established.[9]

Stepwise reduction also causes a lowering of the intensity and the eventual disappearance of the long-wavelength band, while a new absorption around 600 nm emerges during the first and second reductions and then diminishes during the third reduction step. The last reversible reduction step also produces a weak and broad absorption around 1200 nm. No other band with absorptivity $\lambda > 1000$ nm was detected, although the EPR experiments suggest a metal−metal mixed-valent situation for complex ion $\mathbf{1}^{-}$. The ruthenium(II)/catecholato species $\mathbf{1}^{2-}$ and $\mathbf{2}^{2-}$ exhibit MLCT [$d(Ru^{II}) \rightarrow \pi^*(tppz)$] absorptions around 720 nm, with the low energy resulting from the catecholato donor effect on the metals. The NIR absorption for the three-electron-reduction product is typical for the $tppz^{\bullet-}$ chromophore,[7] suggesting the formulation shown in Scheme 1.

Comparison of the Semiquinone (2^n) and Iminosemiquinone (3^n) Redox Series. Although modification of the redox system 2^n, in relation to the previously reported[7c] analogue 3^n with two iminobenzoquinone instead of benzoquinone termini, appears small enough, there are some notable differences. Most importantly, the above-mentioned shift of the redox potentials (Table 3) to significantly more positive values in the all-oxygen-coordinated diruthenium system leads to isolation of the neutral forms **1** and **2**, in contrast to the more accessible dication $\mathbf{3}^{2+}$.[7c] Higher oxidized ($n = 3+, 4+$) states were thus available[7c] for 3^n,

dx.doi.org/10.1021/ic102280q |*Inorg. Chem.* 2011, 50, 4753–4763

Table 7. Main TD-DFT/(U)B3LYP Calculated Transitions of 1

energy (eV)	wavelength (nm)	oscillator strength	transition	character
1.225	1012	0.0106	(85%) SOMO1(α) → LUMO(α)	Q(π) → tppz(π^*) (major)
				Ru(dπ) → tppz(π^*) (minor)
1.297	956	0.0751	(82%) SOMO2(α) → LUMO(α)	Q(π) → tppz(π^*) (major)
				Ru(dπ) → tppz(π^*) (minor)
1.352	917	0.0156	(53%) HOMO−2(α) → LUMO(α)	Ru(dπ) → tppz(π^*)
			(29%) HOMO−1(β) → LUMO(β)	Ru(dπ)/Q(π) → Q(π^*)
2.005	618	0.0645	(49%) HOMO−5(β) → LUMO(β)	Ru(dπ)/Q(π) → Q(π^*)
			(26%) HOMO−4(α) → LUMO(α)	Ru(dπ)/Cl(π) → tppz(π^*)

whereas $\mathbf{1}^{n}$ and $\mathbf{2}^{n}$ can be reduced to the n = 3− forms (Scheme 1). The common 2+ forms exhibit similar absorption maxima around 700 nm and the isolated anti configuration of diamagnetic $\mathbf{3}^{2+}$ can be best described as an antiferromagnetically coupled bis[iminosemiquinonatoruthenium(III)] system. The [1+] intermediates of $\mathbf{1}^{n}$, $\mathbf{2}^{n}$, and $\mathbf{3}^{n}$ exhibit absorption and EPR features comparable with those of a semiquinone-based spin, in agreement with DFT-calculated spin densities (Figure 10 and Table 5).[7c] While the neutral form **3** could not be isolated, the present study reveals not only a specific paramagnetic behavior (as discussed above) but also different long-wavelength absorptions in the form of two very intense and rather narrow bands at about 920 and 615 nm (Figures 11−13 and Table 6). The electrogenerated compound **3** had shown one less intense band at ca. 750 nm.[7c] Like the spin−spin interaction, these absorptions, identified as mainly ligand-to-ligand transitions (Table 7), are presumed to be highly sensitive to the conformation, which is most likely to be affected by steric interference involving the phenylimino group in $\mathbf{3}^{n}$. Replacement of that interfering and mobile NPh function by oxygen leads to more spectacular optical absorption, useful for NIR applications.[26]

CONCLUSION

In summary, we have succeeded in bridging two *o*-semiquinones in the form of stable metal complexes with considerably narrowed frontier orbitals, which leads to intramolecular spin−spin coupling across ca. 1 nm distance, intermolecular magnetic interactions between semiquinone ligands, high-intensity NIR absorption (a sought-after molecular property),[26] and multiple electron-transfer activity within a ca. 1 V range, which allowed for spectroelectrochemical characterization of several charged states. The DFT-supported oxidation state assignments with conceivable alternatives (Scheme 1) can be compared with a related system $[(Q^{\bullet-})RuCl(\mu\text{-tppz})ClRu(Q^{\bullet-})]^{n}$ containing a substituted iminosemiquinone $Q^{\bullet-}$,[7c] revealing correspondences but also differences: As a result of positively shifted redox potentials for the quinone versus iminoquinone systems, it is the *neutral* triplet forms **1** and **2** that are isolated and not the dication, as in $\mathbf{3}^{2+}$.[7c] Oxidation to the mixed-valent trication[7c] was thus not possible here. A further remarkable difference is the stability of iminosemiquinone toward reduction, which, for the monoanion, leads to bis(iminosemiquinonato)diruthenium(II) bridged by $tppz^{\bullet-}$, whereas $\mathbf{2}^{-}$ has mixed catecholato/semiquinonato and $\mathbf{1}^{-}$ exclusively catecholato terminal ligands (and unreduced tppz as a bridge; see Scheme 1). For the redox series presented here, reduction of tppz occurs only *after* the metals and quinone ligands have been reduced to their lowest oxidation levels. While the redox potential shifts (Table 3) for quinone-based electron transfer are as expected, replacement of the popular[8] 4,6-di-*tert*-butyl-*N*-arylimino-*o*-benzoquinone ligands by the *o*-benzoquinone parent systems as in **1** or **2** described here can have additional, less immediately obvious consequences. For a given charge state, the weaker σ-donor capacity of O versus NR analogues, the diminished π overlap,[9a,m,s] and the smaller steric requirements (allowing for closer contact; see Figure 2) can affect intra- and intermolecular magnetic interactions and ligand-based electronic transitions.

EXPERIMENTAL SECTION

Materials. The starting complex $[Cl_3Ru^{III}(\mu\text{-tppz})Ru^{III}Cl_3]$ was prepared according to the reported procedure.[7d] The ligands catechol (H_2Q) and 3,5-di-*tert*-butylcatechol [H_2(DBQ)] were purchased from Aldrich, USA. Other chemicals and solvents were reagent-grade and were used as received. For spectroscopic and electrochemical studies, high-performance liquid chromatography grade solvents were used.

Instrumentation. UV−vis−NIR spectroelectrochemical studies were performed in CH_3CN/0.1 M Bu_4NPF_6 at 298 K using an optically transparent thin-layer electrode cell[27a] mounted in the sample compartment of a J&M TIDAS spectrophotometer. ^{1}H NMR spectra were obtained with a 300 MHz Varian FT spectrometer. EPR measurements were taken in a two-electrode capillary tube[27b] with an X-band Bruker system ESP300, equipped with a Bruker ER035 M gaussmeter and a HP 5350B microwave counter. Cyclic voltammetric, differential pulse voltammetric, and coulometric measurements were carried out using a PAR model 273A electrochemistry system. Platinum wire working and auxiliary electrodes and an aqueous saturated calomel reference electrode were used in a three-electrode configuration. The supporting electrolyte was 0.1 M Et_4NClO_4, and the solute concentration was $\sim 10^{-3}$ M. The half-wave potential E°_{298} was set equal to $0.5(E_{pa} + E_{pc})$, where E_{pa} and E_{pc} are anodic and cathodic cyclic voltammetric peak potentials, respectively. Elemental analyses were carried out with a Perkin-Elmer 240C elemental analyzer. Electrospray mass spectra were recorded on a Micromass Q-ToF mass spectrometer.

Crystallography. Single crystals of **2** were grown by the slow diffusion of its dichloromethane solution into acetonitrile, followed by the slow evaporation of the solvent mixture. X-ray diffraction data were collected using an Oxford XCALIBUR-S CCD single-crystal X-ray diffractometer. The structure was solved and refined by full-matrix least-squares techniques on F^2 using the *SHELX-97* program.[28] The absorption correction was done by the multiscan technique. All data were corrected for Lorentz and polarization effects, and the non-hydrogen atoms were refined anisotropically. Hydrogen atoms were included in the refinement process as per the riding model. **2** crystallized with 1.25 molecules of H_2O and 1 molecule of CH_2Cl_2. The hydrogen atoms associated with the H_2O molecules could not be located.

Magnetic Measurements. The variable-temperature magnetic susceptibilities were measured on polycrystalline samples with a Quantum

dx.doi.org/10.1021/ic102280q |*Inorg. Chem.* 2011, 50, 4753–4763

Design MPMSXL superconducting quantum interference device (SQUID) susceptometer over a temperature range of 2−300 K at constant fields of 0.1, 1, and 5 T. Each raw data set was corrected for the diamagnetic contribution of both the sample holder and the complex to the susceptibility. Molar diamagnetic corrections were calculated on the basis of Pascal constants. Magnetization measurements were carried out at 2 and 300 K from 0 to 5 T. For complex **1**, hysteresis loops between −5 and +5 T at 2 and 300 K were measured. ZFC and FC susceptibilities for **1** were also measured at a magnetic field of 0.1 T from 2 to 300 K. The fitting of the experimental data was carried out using the *MATLAB V.S.1.0.421* program.

Computational Details. Full geometry optimizations were carried out using the DFT method at the B3LYP level.[29] All elements except ruthenium were assigned to the 6-31G(d) basis set. The SDD basis set with effective core potential was employed for the ruthenium atom.[30] The vibrational frequency calculations were performed to ensure that the optimized geometries represent the local minima and there are only positive eigenvalues. All calculations were performed with the *Gaussian03* program package.[31] Vertical electronic excitations based on B3LYP-optimized geometries were computed using the TD-DFT formalism[32] in acetonitrile using a conductor-like polarizable continuum model.[33] GaussSum[34] was used to calculate the fractional contributions of various groups to each molecular orbital.

Synthesis of [{(Q)ClRu^{II}}$_2$(μ-tppz)] (1). The starting complex [Cl_3Ru(μ-tppz)RuCl_3] (100 mg, 0.124 mmol), catechol (H_2Q; 34 mg, 0.31 mmol), excess LiCl (54 mg, 1.3 mmol), and NEt_3 (0.2 mL, 1.55 mmol) were mixed in 20 mL of ethanol, and the mixture was heated to reflux for 3 h under atmospheric conditions. The initial greenish solution gradually changed to deep green. The solvent was then removed under reduced pressure. The dried crude product was purified by using a silica gel column. The green dinuclear complex **1** was eluted by a solvent mixture of CH_3CN/MeOH (6:1). Evaporation of the solvent under reduced pressure yielded pure complex **1**.

Yield: 57 mg (52%). Anal. Calcd (found) $C_{36}H_{24}Cl_2N_6O_4Ru_2$: C, 49.21 (49.09); H, 2.76 (2.82); N, 9.57 (9.43). ESI-MS (in CH_3CN). Calcd (found) for $[\mathbf{1}]^+$: m/z 877.93 (877.03). ^{1}H NMR in $CDCl_3$ (δ, ppm): 22.6 (2H), 21.0 (1H), 20.5 (1H), 13.7 (1H), 12.9 (1H), 8.9 (2H), 8.3 (2H), 6.7 (3H, m), 3.7 (6H, m), −1.2 (1H), −19.3 (2H), −37.6 (2H).

Synthesis of [{(DTBQ)ClRu^{II}}$_2$(μ-tppz)] (2). The starting complex [Cl_3Ru(μ-tppz)RuCl_3] (100 mg, 0.124 mmol), 3,5-di-*tert*-butylcatechol [H_2(DTBQ); 69 mg, 0.31 mmol], excess LiCl (54 mg, 1.3 mmol), and NEt_3 (0.2 mL, 1.55 mmol) were mixed in 20 mL of ethanol, and the mixture was heated to reflux for 4.5 h under atmospheric conditions. The initial greenish solution gradually changed to deep green. The solvent was then removed under reduced pressure. The dried crude product was purified by using a silica gel column. The green dinuclear complex **2** was eluted by a solvent mixture of CH_2Cl_2/CH_3CN (6:1). Evaporation of the solvent under reduced pressure yielded pure complex **2**.

Yield: 65 mg (47%). Anal. Calcd (found) $C_{52}H_{56}Cl_2N_6O_4Ru_2$: C, 56.61 (56.79); H, 5.12 (5.28); N, 7.62 (7.56). ESI-MS (in CH_3CN). Calcd (found) for $[\mathbf{2}]^+$: m/z 1102.18 (1101.83). ^{1}H NMR in $CDCl_3$ (δ, ppm): 20.6 (1H), 18.4 (2H), 14.9 (30H), 10.3 (1H), 9.2 (1H), 6.8 (2H), 4.3 (1H), 3.5 (1H), 2.6 (10H), 1.3 (6H), −3.4 (1H).

■ ASSOCIATED CONTENT

Supporting Information. Calculated bond distances, molecular orbitals, mass spectra, ^{1}H NMR spectra, DFT-optimized structure of **1**, magnetization versus magnetic field plots, magnetic susceptibility, and hysteresis loops. This material is available free of charge via the Internet at http://pubs.acs.org.

■ AUTHOR INFORMATION

Corresponding Author

*E-mail: reyesja@quim.ucm.es (R.J.-A.), kaim@iac.uni-stuttgart.de (W.K.), lahiri@chem.iitb.ac.in (G.K.L.).

■ ACKNOWLEDGMENT

Financial support received from the Department of Science and Technology (New Delhi, India), the DAAD, FCI, and DFG (Germany), GACR (203/09/0705; Czech Republic), Spanish MICINN (CTQ 2008-00920), C.M. (S2009/MAT-1467), and BSCH-UCM (921073-4120824) is gratefully acknowledged. X-ray structural studies for **1** were carried out at the National Single Crystal Diffractometer Facility, Indian Institute of Technology Bombay. Special acknowledgment is made to the Sophisticated Analytical Instrument Facility, Indian Institute of Technology Bombay, for providing the NMR facility.

■ REFERENCES

(1) (a) Kaim, W.; Schwederski, B. *Bioinorganic Chemistry*; Wiley: Chichester, U.K., 1994. (b) Swamy, U.; Wang, M.; Tripathy, J. N.; Kim, S. K.; Hirasawa, M.; Knaff, D. B.; Allen, J. P. *Biochemistry* **2005**, *44*, 16054.

(2) (a) Collman, J. P.; Devaraj, N. K.; Decréau, R. A.; Yang, Y.; Yan, Y.-L.; Ebina, W.; Eberspacher, T. A.; Chidsey, C. E. D. *Science* **2007**, *315*, 1565. (b) Alstrum-Acevedo, J. H.; Brennaman, M. K.; Meyer, T. J. *Inorg. Chem.* **2005**, *44*, 6802. (c) Dempsey, J. L.; Esswein, A. J.; Manke, D. R.; Rosenthal, J.; Soper, J. D.; Nocera, D. G. *Inorg. Chem.* **2005**, *44*, 6879. (d) Stanciu, C.; Jones, M. E.; Fanwick, P. E.; Abu-Omar, M. M. *J. Am. Chem. Soc.* **2007**, *129*, 12400.

(3) (a) Kaim, W.; Schwederski, B. *Coord. Chem. Rev.* **2010**, *254*, 1580. (b) Ward, M. D. *J. Solid State Electrochem.* **2005**, *9*, 778. (c) Griffith, W. P. *Transition Met. Chem.* **1993**, *18*, 250.

(4) (a) Ye, S.; Sarkar, B.; Lissner, F.; Schleid, T.; van Slageren, J.; Fiedler, J.; Kaim, W. *Angew. Chem.* **2005**, *117*, 2140. *Angew. Chem., Int. Ed.* **2005**, *44*, 2103. (b) Chaudhuri, P.; Verani, C. N.; Bill, E.; Bothe, E.; Weyhermüller, T.; Wieghardt, K. *J. Am. Chem. Soc.* **2001**, *123*, 2213.

(5) Muñoz-Castro, A.; MacLeod Carey, D.; Morales-Verdejo, C.; Chávez, I.; Manríquez, J. M.; Arratia-Pérez, R. *Inorg. Chem.* **2010**, *49*, 4175.

(6) (a) Qian, G.; Wang, Z. Y. *Chem. Asian J.* **2010**, *5*, 1006. (b) Grätzel, M. *J. Photochem. Photobiol. C: Photochem. Rev.* **2003**, *4*, 145. (c) Marshall, K. L.; Painter, G.; Lotito, K.; Noto, A. G.; Chang, P. *Mol. Cryst. Liq. Cryst.* **2006**, *454*, 47. (d) Thorley, K. J.; Hales, J. M.; Anderson, H. L.; Perry, J. W. *Angew. Chem., Int. Ed.* **2008**, *47*, 7095. (e) Blanco, M.; Villarroya, I. *Trends Anal. Chem.* **2002**, *21*, 240. (f) Zhao, W.; Carreira, E. M. *Angew. Chem., Int. Ed.* **2005**, *44*, 1677. (g) Garreau-de Bonneval, B.; Moineau-Chane Ching, K. I.; Alary, F.; Bui, T.-T.; Valade, L. *Coord. Chem. Rev.* **2010**, *254*, 1457. (h) Deplano, P.; Mercuri, M. L.; Pintus, G.; Trogu, E. F. *Comments Inorg. Chem.* **2001**, *22*, 353.

(7) (a) Ghumaan, S.; Sarkar, B.; Chanda, N.; Sieger, M.; Fiedler, J.; Kaim, W.; Lahiri, G. K. *Inorg. Chem.* **2006**, *45*, 7955. (b) Koley, M.; Sarkar, B.; Ghumaan, S.; Bulak, E.; Fiedler, J.; Kaim, W.; Lahiri, G. K. *Inorg. Chem.* **2007**, *46*, 3736. (c) Das, A. K.; Sarkar, B.; Fiedler, J.; Záliš, S.; Hartenbach, I.; Strobel, S.; Lahiri, G. K.; Kaim, W. *J. Am. Chem. Soc.* **2009**, *131*, 8895. (d) Hartshorn, V.; Daire, N.; Tondreau, V.; Loeb, B.; Meyer, T. J.; White, P. S. *Inorg. Chem.* **1999**, *38*, 3200. (e) Chanda, N.; Laye, R. H.; Chakraborty, S.; Paul, R. L.; Jeffery, J. C.; Ward, M. D.; Lahiri, G. K. *J. Chem. Soc., Dalton Trans.* **2002**, 3496. (f) Rocha, R. C.; Rein, F. N.; Jude, H.; Shreve, A. P.; Concepcion, J. J.; Meyer, T. J. *Angew. Chem., Int. Ed.* **2008**, *47*, 503. (g) Wadman, S. H.; Havenith, R. W. A.; Hartl, F.; Lutz, M.; Spek., A. L.; van Klink, G. P. M.; van Koten, G. *Inorg. Chem.* **2009**, *48*, 5685. (h) Bernhard, S.; Takada, K.; Diaz, D. J.; Abruña, H. D.; Mürne, H. *J. Am. Chem. Soc.* **2001**, *123*, 10265. (i) Kundu, T.;

Sarkar, B.; Mondal, T. K.; Fiedler, J.; Mobin, S. M.; Kaim, W.; Lahiri, G. K. *Inorg. Chem.* **2010**, *49*, 6565.

(8) Poddelsky, A. I.; Cherkasov, V. V.; Abakumov, G. A. *Coord. Chem. Rev.* **2009**, *253*, 291.

(9) (a) Lever, A. B. P. *Coord. Chem. Rev.* **2010**, *254*, 1397. (b) Patra, S.; Sarkar, B.; Mobin, S. M.; Kaim, W.; Lahiri, G. K. *Inorg. Chem.* **2003**, *42*, 6469. (c) Ernst, S.; Kasack, V.; Bessenbacher, C.; Kaim, W. *Z. Naturforsch.* **1987**, *42b*, 425. (d) Ernst, S.; Hänel, P.; Jordanov, J.; Kaim, W.; Kasack, V.; Roth, E. *J. Am. Chem. Soc.* **1989**, *111*, 1733. (e) Patra, S.; Sarkar, B.; Ghumaan, S.; Fiedler, J.; Záliš, S.; Kaim, W.; Lahiri, G. K. *Dalton Trans.* **2004**, 750. (f) Ye, S.; Sarkar, B.; Duboc, C.; Fiedler, J.; Kaim, W. *Inorg. Chem.* **2005**, *44*, 2843. (g) Maji, S.; Sarkar, B.; Mobin, S. M.; Fiedler, J.; Urbanos, F. A.; Jimenez-Aparicio, R.; Kaim, W.; Lahiri, G. K. *Inorg. Chem.* **2008**, *47*, 5204. (h) Ghumaan, S.; Sarkar, B.; Maji, S.; Puranik, V. G.; Fiedler, J.; Urbanos, F. A.; Jimenez-Aparicio, R.; Kaim, W.; Lahiri, G. K. *Chem.—Eur. J.* **2008**, *14*, 10816. (i) Das, A. K.; Sarkar, B.; Duboc, C.; Strobel, S.; Fiedler, J.; Záliš, S.; Lahiri, G. K.; Kaim, W. *Angew. Chem.* **2009**, *121*, 4306. *Angew. Chem., Int. Ed.* **2009**, *48*, 4242. (j) Chatterjee, S.; Singh, P.; Fiedler, J.; Baková, R.; Zališ, S.; Kaim, W.; Goswami, S. *Dalton Trans.* **2009**, 7778. (k) Haga, M.; Dodsworth, E. S.; Lever, A. B. P. *Inorg. Chem.* **1986**, *25*, 447. (l) Masui, H.; Lever, A. B. P.; Auburn, P. *Inorg. Chem.* **1991**, *30*, 2402. (m) Ebadi, M.; Lever, A. B. P. *Inorg. Chem.* **1999**, *38*, 467. (n) Lever, A. B. P.; Auburn, P. R.; Dodsworth, E. S.; Haga, M.; Liu, W.; Melnik, M.; Nevin, W. A. *J. Am. Chem. Soc.* **1988**, *110*, 8076. (o) Auburn, P. R.; Dodsworth, E. S.; Haga, M.; Liu, W.; Nevin, W. A.; Lever, A. B. P. *Inorg. Chem.* **1991**, *30*, 3502. (p) Lever, A. B. P.; Gorelsky, S. L. *Struct. Bonding (Berlin)* **2004**, *107*, 77. (q) Haga, M.; Dodsworth, E. S.; Lever, A. B. P.; Boone, S. R.; Pierpont, C. G. *J. Am. Chem. Soc.* **1986**, *108*, 7413. (r) Meacham, A. P.; Druce, K. L.; Bell, Z. R.; Ward, M. D.; Keister, J. B.; Lever, A. B. P. *Inorg. Chem.* **2003**, *42*, 7887. (s) Kalinina, D.; Dares, D.; Kaluarachchi, H.; Potvin, P. G.; Lever, A. B. P. *Inorg. Chem.* **2008**, *47*, 10110. (t) Kumbhakar, D.; Sarkar, B.; Das, A.; Das, A. K.; Mobin, S. M.; Fiedler, J.; Kaim, W.; Lahiri, G. K. *Dalton Trans.* **2009**, 9645. (u) Muckerman, J. T.; Polyansky, D. E.; Wada, T.; Tanaka, K.; Fujita, E. *Inorg. Chem.* **2008**, *47*, 1787. (v) Tsai, M.-K.; Rochford, J.; Polyansky, D. E.; Wada, T.; Tanaka, K.; Fujita, E.; Muckerman, J. T. *Inorg. Chem.* **2009**, *48*, 4372.

(10) Remenyi, C.; Kaupp, M. *J. Am. Chem. Soc.* **2005**, *127*, 11399.

(11) Boyer, J. L.; Rochford, J.; Tsai, M.-K.; Muckerman, J. T.; Fujita, E. *Coord. Chem. Rev.* **2010**, *254*, 309.

(12) (a) Patra, S.; Miller, T. A.; Sarkar, B.; Niemeyer, M.; Ward, M. D.; Lahiri., G. K. *Inorg. Chem.* **2003**, *42*, 4707. (b) Koiwa, T.; Masuda, Y.; Shono, J.; Kawamoto, Y.; Hoshino, Y.; Hashimoto, T.; Natarajan, K.; Shimizu, K. *Inorg. Chem.* **2004**, *43*, 6215. (c) Eaton, D. R. *J. Am. Chem. Soc.* **1965**, *87*, 3097. (d) Palmer, R. A.; Fay, R. C.; Piper, T. S. *Inorg. Chem.* **1964**, *3*, 875. (e) Holm, R. H.; Cotton, F. A. *J. Am. Chem. Soc.* **1958**, *80*, 5658. (f) Fay, R. C.; Piper, T. S. *J. Am. Chem. Soc.* **1963**, *85*, 500. (g) Chen, J.-L.; Zhang, X.-U.; Zhang, L.-Y.; Shi, L.-X.; Chen, Z.-N. *Inorg. Chem.* **2005**, *44*, 1037.

(13) Bhattacharya, S.; Gupta, P.; Basuli, F.; Pierpont, C. G. *Inorg. Chem.* **2002**, *41*, 5810.

(14) Kahn, O. *Molecular Magnetism*; VCH Publishers, Inc.: New York, 1993; p 107.

(15) (a) Barral, M. C.; Gallo, T.; Herrero, S.; Jiménez-Aparicio, R.; Torres, M. R.; Urbanos, F. A. *Inorg. Chem.* **2006**, *45*, 3639. (b) Liu, W.; Nfor, E. N.; Li, Y. Z.; Zuo, J. L.; You, X. Z. *Inorg. Chem. Commun.* **2006**, *9*, 923. (c) Dikarev, E. V.; Filatov, A. S.; Clérac, R.; Petrukhina, M. A. *Inorg. Chem.* **2006**, *45*, 744. (d) Motokawa, N.; Oyama, T.; Matsunaga, S.; Miyasaka, H.; Sugimoto, K.; Yamashita, M.; Lopez, N.; Dunbar, K. R. *Dalton Trans.* **2008**, 4099.

(16) Barral, M. C.; Gonzalez-Prieto, R.; Jiménez-Aparicio, R.; Priego, J. L.; Torres, M. A.; Urbanos, F. A. *Eur. J. Inorg. Chem.* **2003**, 2339.

(17) (a) Lucas, C. R.; Liu, S. *Inorg. Chem.* **1997**, *36*, 4336. (b) Cukiernik, F. D.; Luneau, D.; Marchon, J. C.; Maldivi, P. *Inorg. Chem.* **1998**, *37*, 3698. (c) Jiménez-Aparicio, R.; Urbanos, F. A.; Arrieta, J. M. *Inorg. Chem.* **2001**, *40*, 613. (d) Lee, E. W.; Kim, Y. J.; Jung, D. Y. *Inorg. Chem.* **2002**, *41*, 501. (e) Wang, C. F.; Zuo, J. L.; Ying, J. W.; Ren, T.; You, X. Z. *Inorg. Chem.* **2008**, *47*, 9716. (f) Trtica, S.; Prosenc, M. H.; Schmidt, M.; Heck, J.; Albrecht, O.; Görlitz, D.; Reuter, F.; Rentschler, E. *Inorg. Chem.* **2010**, *49*, 1667. (g) Bauer, E. M.; Bellitto, C.; Imperatori, P.; Righini, G.; Colapietro, M.; Portalone, G.; Gómez-García, C. J. *Inorg. Chem.* **2010**, *49*, 7472.

(18) Lange, C. W.; Conklin, B. J.; Pierpont, C. G. *Inorg. Chem.* **1994**, *33*, 1276.

(19) O'Connor, C. J. *Prog. Inorg. Chem.* **1982**, *29*, 203.

(20) Das, D.; Das, A. K.; Sarkar, B.; Mondal, T. K.; Mobin, S. M.; Fiedler, J.; Záliš, S.; Urbanos, F. A.; Jiménez-Aparicio, R.; Kaim, W.; Lahiri, G. K. *Inorg. Chem.* **2009**, *48*, 11853.

(21) Hatscher, S.; Schilder, H.; Lueken, H.; Urland, W. *Pure Appl. Chem.* **2005**, *77*, 497.

(22) (a) Carlin, R. L. *Magnetochemistry*; Springer-Verlag: Berlin, 1986; p 148. (b) Kahn, O. *Molecular Magnetism*; VCH Publishers, Inc.: New York, 1993; p 321.

(23) (a) Kennon, B. S.; Her, J. H.; Stephens, P. W.; Miller, J. S. *Inorg. Chem.* **2009**, *48*, 6117. (b) Li, Z. X.; Zhao, J. P.; Sañudo, E. C.; Ma, H.; Pan, Z. D.; Zeng, Y. F.; Bu, X. H. *Inorg. Chem.* **2009**, *48*, 11601. (c) Luneau, D.; Borta, A.; Chumakov, Y.; Jacquot, J. F.; Erwann Jeanneau, E.; Lescop, C.; Rey, P. *Inorg. Chim. Acta* **2008**, *361*, 3669. (d) Zhang, J. Y.; Liu, C. M.; Zhang, D. Q.; Gao, S.; Zhu, D. B. *Inorg. Chem. Commun.* **2007**, *10*, 897. (e) Zheng, L. M.; Gao, S.; Yin, P.; Xin, X. Q. *Inorg. Chem.* **2004**, *43*, 2151.

(24) (a) Kaim, W.; Fiedler, J. *Chem. Soc. Rev.* **2009**, *38*, 3373. (b) Kaim, W. In *Discussion Meeting on Electroanalytical Techniques and Their Applications (DM-ELANTE-2008)*; Aggarwal, S. K., Gopinath, N., Govindan, R., Sawant, R. M., Eds.; Indian Society for Electroanalytical Chemistry: Mumbai, India, 2008; p 35.

(25) Roy, S.; Sarkar, B.; Bubrin, D.; Niemeyer, M.; Zališ, S.; Lahiri, G. K.; Kaim, W. *J. Am. Chem. Soc.* **2008**, *130*, 15230.

(26) Kaim, W. *Coord. Chem. Rev.* DOI: 10.1016/j.ccr.2011.01.014.

(27) (a) Krejcik, M.; Danek, M.; Hartl, F. *J. Electroanal. Chem.* **1991**, *317*, 179. (b) Kaim, W.; Ernst, S.; Kasack, V. *J. Am. Chem. Soc.* **1990**, *112*, 173.

(28) Sheldrick, G. M. *SHELX-97, Program for Crystal Structure Solution and Refinement*; University of Göttingen:Göttingen, Germany, 1997.

(29) Lee, C.; Yang, W.; Parr, R. G. *Phys. Rev. B* **1988**, *37*, 785.

(30) (a) Andrae, D.; Haeussermann, U.; Dolg, M.; Stoll, H.; Preuss, H. *Theor. Chim. Acta* **1990**, *77*, 123. (b) Fuentealba, P.; Preuss, H.; Stoll, H.; Szentpaly, L. V. *Chem. Phys. Lett.* **1989**, *89*, 418.

(31) Frisch, M. J.; Trucks, G. W.; Schlegel, H. B.; Scuseria, G. E.; Robb, M. A.; Cheeseman, J. R.; Montgomery, J. A., Jr.; Vreven, T.; Kudin, K. N.; Burant, J. C.; Millam, J. M.; Iyengar, S. S.; Tomasi, J.; Barone, V.; Mennucci, B.; Cossi, M.; Scalmani, G.; Rega, N.; Petersson, G. A.; Nakatsuji, H.; Hada, M.; Ehara, M.; Toyota, K.; Fukuda, R.; Hasegawa, J.; Ishida, M.; Nakajima, T.; Honda, Y.; Kitao, O.; Nakai, H.; Klene, M.; Li, X.; Knox, J. E.; Hratchian, H. P.; Cross, J. B.; Bakken, V.; Adamo, C.; Jaramillo, J.; Gomperts, R.; Stratmann, R. E.; Yazyev, O.; Austin, A. J.; Cammi, R.; Pomelli, C.; Ochterski, J. W.; Ayala, P. Y.; Morokuma, K.; Voth, G. A.; Salvador, P.; Dannenberg, J. J.; Zakrzewski, V. G.; Dapprich, S.; Daniels, A. D.; Strain, M. C.; Farkas, O.; Malick, D. K.; Rabuck, A. D.; Raghavachari, K.; Foresman, J. B.; Ortiz, J. V.; Cui, Q.; Baboul, A. G.; Clifford, S.; Cioslowski, J.; Stefanov, B. B.; Liu, G.; Liashenko, A.; Piskorz, P.; Komaromi, I.; Martin, R. L.; Fox, D. J.; Keith, T.; Al-Laham, M. A.; Peng, C. Y.; Nanayakkara, A.; Challacombe, M.; Gill, P. M. W.; Johnson, B.; Chen, W.; Wong, M. W.; Gonzalez, C.; Pople, J. A. *Gaussian 03*; Gaussian, Inc.: Wallingford, CT, 2004.

(32) (a) Bauernschmitt, R.; Ahlrichs, R. *Chem. Phys. Lett.* **1996**, *256*, 454. (b) Stratmann, R. E.; Scuseria, G. E.; Frisch, M. J. *J. Chem. Phys.* **1998**, *109*, 8218. (c) Casida, M. E.; Jamorski, C.; Casida, K. C.; Salahub, D. R. *J. Chem. Phys.* **1998**, *108*, 4439.

(33) (a) Barone, V.; Cossi, M. *J. Phys. Chem. A* **1998**, *102*, 1995. (b) Cossi, M.; Barone, V. *J. Chem. Phys.* **2001**, *115*, 4708. (c) Cossi, M.; Rega, N.; Scalmani, G.; Barone, V. *J. Comput. Chem.* **2003**, *24*, 669.

(34) O'Boyle, N. M.; Tenderholt, A. L.; Langner, K. M. *J. Comput. Chem.* **2008**, *29*, 839.